

Coarse-Grained Picture for Controlling Quantum Chaos

Toshiya TAKAMI

Institute for Molecular Science, Okazaki 444-8585, Japan

Hiroshi FUJISAKI

Department of Chemistry, Boston University, 590 Commonwealth Ave., Boston, Massachusetts, 02215, USA

Takayuki MIYADERA

Department of Information Sciences, Tokyo University of Science, Noda City, 278-8510, Japan

(Dated: November 2, 2018)

We propose a coarse-grained picture to analyze control problems for quantum chaos systems. Using optimal control theory, we first show that almost perfect control is achieved for random matrix systems and a quantum kicked rotor. Second, under the assumption that the controlled dynamics is well described by a Rabi-type oscillation between unperturbed states, we derive an analytic expression for the optimal field. Finally we numerically confirm that the analytic field can steer an initial state to a target state in random matrix systems.

Keywords: Rabi frequency, optimal control theory, random matrix, kicked rotor, quantum chaos, coarse grain

I. INTRODUCTION

Controlling quantum systems is one of hot topics in physics and chemistry as illustrated in the fields of quantum information processings [1, 2, 3] and laser control of atomic and molecular processes [4]. As for the latter, there have been devised various control schemes: A π -pulse is a simple example to induce a transition between two eigenstates [5]. As a generalization of the π pulse or adiabatic rapid passage [6], we can utilize the nonadiabatic transitions induced by laser fields [7]. For more than three level systems, STIRAP scheme uses a counterintuitive pulse sequence to achieve a perfect population transfer between two eigenstates [8]. When more than two electronic states are involved in the controlled system, we can use a pulse-timing control (Tannor-Rice) scheme to selectively break a chemical bond on a desired potential surface by using a pump and dump pulses with an appropriate time interval [9]. When the controlled system has more than two pathways from an initial state to a target state, quantum mechanical interference between them can be utilized to modify the ratio of products, which is called coherent control (Shapiro-Brumer) scheme [10].

These control schemes are very effective for a certain class of processes but are not versatile and ineffective for, e.g., multi-level-multi-level transitions we shall consider in this paper. There exist several mathematical studies which investigate controllability of general quantum-mechanical systems [11, 12]. The theorem of controllability says that quantum mechanical systems with a discrete spectrum under certain conditions have complete controllability in the sense that an initial state can be guided to a chosen target state after some time. Although the theorem guarantees the existence of optimal fields, it does not tell us how to construct such a field for a given problem.

One of the method to practically design an optimal field is optimal control theory (OCT) [12, 13] or genetic

algorithms [4, 14]. We focus on the former in this paper as a theoretical vehicle. The equations derived from OCT are highly nonlinear (and coupled), so we must solve them using some iterative procedures. There are known some effective algorithms to carry out this procedure numerically, however, the field thus obtained is so complicated that it is difficult to analyze the results: What kinds of dynamical processes are involved in the controlled dynamics? In addition, the cost of the computation becomes larger if we want to apply OCT to realistic problems with many degrees of freedom. Several efforts have been paid to reduce computational costs; Zhu and Rabitz [15] have introduced a non-iterative algorithm for the optimal field.

On the other hand, we know that some chemical reaction systems, especially when highly excited, exhibit quantum chaotic features [16], i.e., statistical properties of eigen-energies and eigen-vectors are very similar to those of random matrix systems [17]. We call such systems *quantum chaos systems* in short. It has been also studied how these quantum chaos systems behave under some external parameters [18, 19, 20]. These statistical properties of quantum chaos systems stem from multi-level-multi-level interactions of eigenstates, which are related to the existence of many avoided crossings [21]. Hence it is necessary to consider the interaction between many eigenstates when we study dynamics in such a system. Furthermore, if our purpose is to control a Gaussian wavepacket in a quantum chaos system, the process also becomes a multi-level-multi-level transition because a Gaussian wavepacket in such a system contains many eigenstates. These are our motivations why we treat multi-level-multi-level transitions and want to control them.

This paper is organized as follows. In Sec. II, we show how quantum chaos systems can be controlled under the optimal fields obtained by OCT. The examples are a random matrix system and a quantum kicked ro-

tor. (The former is considered as a strong-chaos-limit case and the latter as mixed regular-chaotic cases.) In Sec. III, a ‘‘coarse-grained’’ Rabi state is introduced to analyze the controlled dynamics in quantum chaos systems. We numerically obtain a smooth transition between time-dependent states, which justifies the use of such a picture. In Sec. IV, we derive an analytic expression for the optimal field under the assumption of the CG Rabi state, and numerically show that the field can really steer an initial state to a target state in random matrix systems. Finally, we summarize the paper and discuss further aspects of controlling quantum chaos.

II. OPTIMAL CONTROL OF QUANTUM CHAOS

We study optimal control problems of quantum chaos systems. Our goal of control is to obtain an optimal field $\varepsilon(t)$ which guides a quantum chaos system from an initial state $|\varphi_i\rangle$ at $t = 0$ to a given target state $|\varphi_f\rangle$ at some specific time $t = T$. One such method is optimal control theory (OCT), which has been successfully applied to atomic and molecular systems [4].

OCT is usually formulated as a variational problem under constraints as follows: We start from the following functional used by Zhu-Botina-Rabitz [13]

$$J = J_0 - \alpha \int_0^T [\varepsilon(t)]^2 dt - 2\text{Re} \left[\langle \phi(T) | \varphi_f \rangle \int_0^T \langle \chi(t) | \frac{\partial}{\partial t} - \frac{H[\varepsilon(t)]}{i\hbar} | \phi(t) \rangle dt \right] \quad (1)$$

The first term in the right-hand side is the squared absolute value of the final overlap,

$$J_0 = |\langle \phi(T) | \varphi_f \rangle|^2. \quad (2)$$

The second term is the penalty term with respect to an amplitude of the external field $\varepsilon(t)$. The factor $\langle \phi(T) | \varphi_f \rangle$ in the last term is introduced to decouple the conditions for the state $|\phi(t)\rangle$ and the inversely-evolving state $|\chi(t)\rangle$, which both evolve under the Hamiltonian $H[\varepsilon(t)]$ [4, 13]. The variation of J with respect to $|\phi(t)\rangle$ and $|\chi(t)\rangle$ gives Schrödinger’s equations,

$$i\hbar \frac{d}{dt} |\phi(t)\rangle = H[\varepsilon(t)] |\phi(t)\rangle, \quad (3)$$

$$i\hbar \frac{d}{dt} |\chi(t)\rangle = H[\varepsilon(t)] |\chi(t)\rangle. \quad (4)$$

Here we impose the following boundary conditions

$$|\phi(0)\rangle = |\varphi_i\rangle, \quad |\chi(T)\rangle = |\varphi_f\rangle. \quad (5)$$

Another variation of J with respect to $\varepsilon(t)$ gives an expression for the external field

$$\varepsilon(t) = \frac{1}{\alpha\hbar} \text{Im} \left[\langle \phi(t) | \chi(t) \rangle \langle \chi(t) | \frac{\partial H[\varepsilon(t)]}{\partial \varepsilon(t)} | \phi(t) \rangle \right]. \quad (6)$$

In actual numerical calculations, we usually solve these equations with some iteration procedure [13] because they are nonlinear with respect to $|\phi(t)\rangle$ and $|\chi(t)\rangle$. The optimal field, Eq. (6), is finally given after a local maximum of the functional is reached.

In the following subsections, we numerically demonstrate to control multi-level-multi-level transition problems in quantum chaos systems: one is a random matrix system, and the other is a quantum kicked rotor.

A. Controlled Random Matrix System

The random matrix was first introduced by E.P. Wigner as a model to mimick unknown interactions in nuclei, and has been studied to describe statistical natures of spectral fluctuations in quantum chaos systems [17]. Here, we introduce a random matrix system driven by a time-dependent external field $\varepsilon(t)$, which is considered as a model of highly excited atoms or molecules under an electromagnetic field. We write the Hamiltonian

$$H[\varepsilon(t)] = H_0 + \varepsilon(t)V \quad (7)$$

where H_0 and V are $N \times N$ random matrices subject to the Gaussian Orthogonal Ensemble (GOE), which represent generic quantum systems with time-reversal symmetry. The matrix elements of H_0 and V are scaled so that the nearest-neighbor spacing of eigenvalues of H_0 and the variance of the off-diagonal elements of V become both unity.

Once we fix the initial state $|\varphi_i\rangle$ and the final state $|\varphi_f\rangle$, the optimal field $\varepsilon(t)$ is obtained by some numerical procedures for appropriate values of the target time T and the penalty factor α . Though there should be many situations corresponding to the choice of $|\varphi_i\rangle$ and $|\varphi_f\rangle$, we only consider the case where they are *Gaussian random vectors*. It is defined by

$$|\varphi\rangle = \sum_j c_j |\phi_j\rangle, \quad (8)$$

where c_j are complex numbers determined from the following Gaussian distribution,

$$P(c_j) \propto \exp(-|c_j|^2), \quad (9)$$

and $|\phi_j\rangle$ is an orthonormal basis.[33] We take this state because it is typical in a random matrix system.

We show two numerical examples for a 64×64 random matrix Hamiltonian: One is the relatively short-time case with $T = 20$ and $\alpha = 1$ shown in Fig. 1, and the other is the case with $T = 200$ and $\alpha = 10$ shown in Fig. 2. In both cases, we obtain the optimal field $\varepsilon(t)$ after 100 iterations using the Zhu-Botina-Rabitz (ZBR) scheme [13] with $\varepsilon(t) = 0$ as an initial guess of the field. The initial and the target state is chosen as Gaussian random vectors as mentioned above. The final overlaps are $J_0 = 0.971$ and 0.982 , respectively.

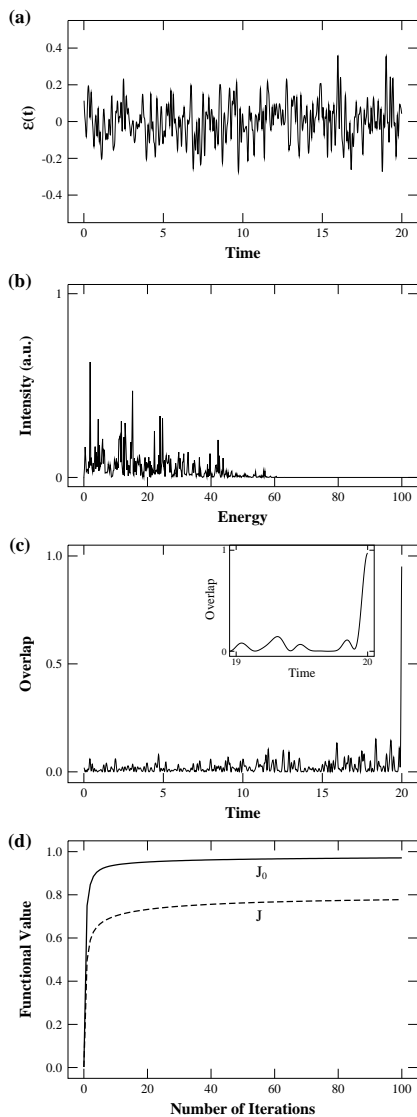


FIG. 1: Optimal Control between Gaussian random vectors in a 64×64 random matrix system by the Zhu-Botina-Rabitz scheme with $T = 20$ and $\alpha = 1$: (a) the optimal field after 100 iterations; (b) its power spectrum; (c) the optimal evolution of the squared overlap with the target $|\langle \phi(t) | \varphi_f \rangle|^2$ as well as its magnified values near the target time in the inset; (d) the convergence behavior of the overlap J_0 (solid) and the functional J (dashed) versus the number of iteration steps.

One sees that the ZBR scheme is effective enough for random matrix systems, i.e., the optimal fields can be obtained even for this type of complicated problems of multi-level-multi-level transitions. However, it seems that the further analysis is difficult because the power spectra for the optimal fields, Figs. 1(b) and 2(b), are very “complex”, i.e., they contain many frequency components.[34]

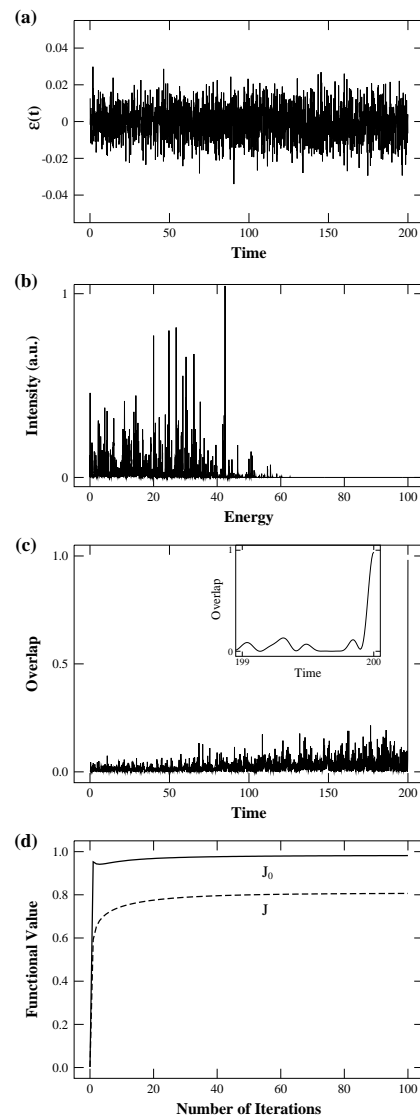


FIG. 2: Optimal Control between Gaussian random vectors in a 64×64 random matrix system by the Zhu-Botina-Rabitz scheme with $T = 200$ and $\alpha = 10$: (a) the optimal field after 100 iterations; (b) its power spectrum; (c) the optimal evolution of the squared overlap with the target, $|\langle \phi(t) | \varphi_f \rangle|^2$ as well as its magnified values near the target time in the inset; (d) the convergence behavior of the overlap J_0 (solid) and the functional J (dashed) versus the number of iteration steps.

B. Controlled Quantum Kicked Rotor

The kicked rotor (or the standard map) is one of famous models in chaotic dynamical systems, and has been studied in various situations [17]. One feature of its chaotic dynamics is the *deterministic diffusion* along the momentum direction. It is also well known that, if we quantize this system, this diffusion is suppressed by the effects of the wavefunction localization in momentum

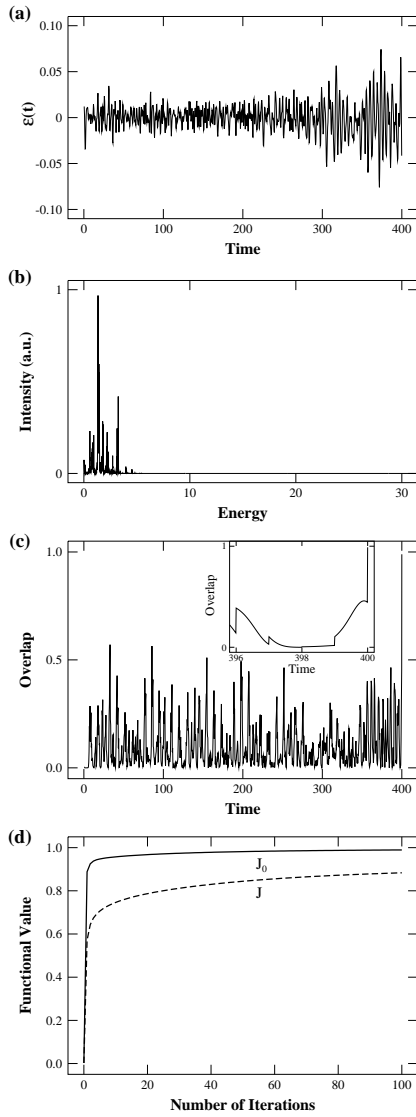


FIG. 3: Optimal Control in a regular kicked rotor with $K = 1$ and $\hbar = 0.3436$ by the Zhu-Botina-Rabitz scheme with $T = 400$ and $\alpha = 1$: (a) the optimal field after 100 iterations; (b) its power spectrum; (c) the optimal evolution of the squared overlap with the target $|\langle \phi(t) | \varphi_f \rangle|^2$ as well as its magnified values near the target time in the inset; (d) the convergence behavior of the overlap J_0 (solid) and the functional J (dashed) versus the number of iteration steps.

space [16].

Here we employ the quantum kicked rotor as a simple model of quantum chaos systems. The Hamiltonian of a kicked rotor is written as

$$H_{\text{KR}}(t) = \frac{p^2}{2} + \frac{K}{\tau} \cos \theta \sum_{n=-\infty}^{\infty} \delta(t - n\tau), \quad (10)$$

where θ is an angle (mod 2π), p momentum, K a kick strength, and τ a period between kicks. An external field

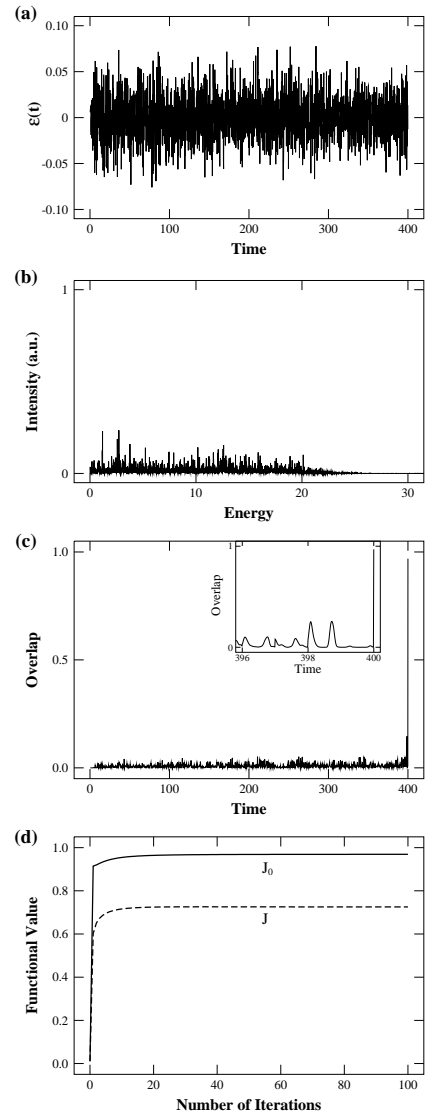


FIG. 4: Optimal Control in a chaotic kicked rotor with $K = 7$ and $\hbar = 0.3436$ by the Zhu-Botina-Rabitz scheme with $T = 400$ and $\alpha = 1$: (a) the optimal field after 100 iterations; (b) its power spectrum; (c) the optimal evolution of the squared overlap with the target, $|\langle \phi(t) | \varphi_f \rangle|^2$ as well as its magnified values near the target time in the inset; (d) the convergence behavior of the overlap J_0 (solid) and the functional J (dashed) versus the number of iteration steps.

$\varepsilon(t)$ is applied through the coupling Hamiltonian

$$H_I[\varepsilon(t)] = -\mu(\theta)\varepsilon(t), \quad (11)$$

where the dipole moment is assumed to be

$$\mu(\theta) = -\cos(\theta + \delta\theta_0). \quad (12)$$

The extra phase $\delta\theta_0$ is introduced to break symmetry of the system. We take $\delta\theta_0 = \pi/3$ in the numerical calculations throughout this paper. The total Hamiltonian is

given by

$$H[\varepsilon(t)] = H_{\text{KR}}(t) + H_{\text{I}}[\varepsilon(t)]. \quad (13)$$

For easiness of computation, we impose a periodic boundary condition for p as well as θ ; the phase space of the corresponding classical system becomes a two-dimensional torus [22, 23]. In this case, Planck's constant is given by $\hbar = 2\pi M/\tau N$, where $p = \pm M\pi$ defines the periodic boundaries in the momentum space, and N is the number of discrete points describing θ and p . In the actual calculations, we set $\tau = 1$.

The kicked rotor is often described only at discrete time immediately after/before the periodic kicks. In our control problem, however, we must represent dynamics driven by $\varepsilon(t)$ between those kicks. Then, we can apply Zhu-Botina-Rabitz scheme as usual. According to Eq. (6), the optimal external field is given by

$$\varepsilon(t) = -\frac{1}{\alpha\hbar} \text{Im} [\langle \phi(t) | \chi(t) \rangle \langle \chi(t) | \mu(\theta) | \phi(t) \rangle]. \quad (14)$$

Note that, because $\mu(\theta)$ commutes with the unitary operator $e^{-iK \cos \theta/\hbar}$ of a kick, $\varepsilon(t)$ is obtained as a continuous function of time even at the moment of the delta kicks.

In Figs. 3 and 4, we show numerical results for the quantum kicked rotor[35] as in Sec. II A. The system parameters are chosen to pick up a regular dynamics (Fig. 3) and a chaotic dynamics (Fig. 4), and the others are $T = 400$ and $\alpha = 1$. The optimal field after 100 iterations for the regular case, Fig. 3(a), is rather simpler than that for the chaotic case, Fig. 4(a). [See also Fig. 3(b) and 4(b).] This is because more states are involved in the latter chaotic process.

Next we investigate the wavepacket dynamics in phase space using the Husimi representation [24]. The initial and final states, $|\varphi_i\rangle$ and $|\varphi_f\rangle$, are chosen as minimum uncertainty (Gaussian) packets centered at (θ_i, p_i) and (θ_f, p_f) , respectively. In Fig. 5(a), we show the result for the regular case corresponding to Fig. 3. Optimal control is achieved for a wavepacket motion within a torus with $J_0 = 0.989$. [36] Figure 5(b) shows the controlled dynamics for the chaotic case corresponding to Fig. 4. In this case, the wavepacket once spreads all over the phase space due to the chaotic nature of the system, but it gets together at the target time T with $J_0 = 0.969$. In both regular and chaotic cases, the ZBR-OCT scheme works well for the quantum kicked rotor [25].

III. COARSE-GRAINED PICTURE

If we apply a resonant external field to a two-level system, we can observe a Rabi oscillation. In such a case, the quantum state is well described by

$$|\phi(t)\rangle = e^{E_1 t/i\hbar} |\phi_1\rangle \cos |\Omega|t - i e^{-i\theta} e^{E_2 t/i\hbar} |\phi_2\rangle \sin |\Omega|t, \quad (15)$$

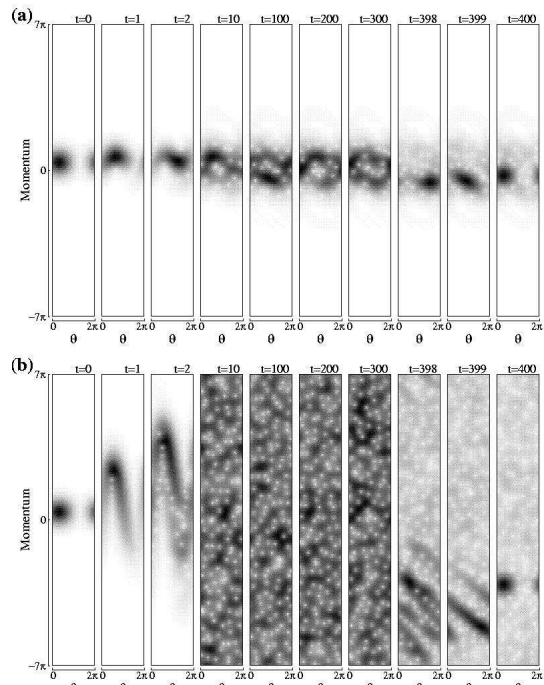


FIG. 5: Time evolution of the Husimi distribution for quantum kicked rotors with $\hbar = 0.3436$ under an optimal field after 100 iterations. The Zhu-Botina-Rabitz scheme was used with the penalty factor $\alpha = 1$ and the target time $T = 400$. From left to right, quantum states immediately after the kick at $t = 0, 1, 2, 10, 100, 200, 300, 398, 399,$ and 400 are depicted. (a) The parameters are $K = 1$ (regular case), $(\theta_i, p_i) = (1.0, 1.0)$ and $(\theta_f, p_f) = (1.0, -1.0)$; (b) $K = 7$ (chaotic case), $(\theta_i, p_i) = (1.0, 1.0)$ and $(\theta_f, p_f) = (1.0, -10.0)$.

where $|\phi_1\rangle$ and $|\phi_2\rangle$ (E_1 and E_2) are two eigenstates (eigen-energies) of the system, $|\Omega| \equiv |\varepsilon_0 \mu_{12}|/\hbar$ the Rabi frequency, $\mu_{12} \equiv \langle \phi_1 | \hat{\mu} | \phi_2 \rangle$ matrix elements of a dipole operator $\hat{\mu}$, ε_0 an amplitude of the field, and θ a certain phase parameter.

In this section, we study the controlled dynamics from an initial state $|\varphi_i\rangle$ at $t = 0$ to a target state $|\varphi_f\rangle$ at $t = T$ in a multi-state quantum mechanical system described by Eq. (7). By introducing a ‘‘coarse-grained’’ picture, which means neglecting highly oscillating terms as the case of rotating-wave approximation (RWA) [5] and assuming that $|\varphi_i\rangle$ and $|\varphi_f\rangle$ contain many eigenstates without any correlation between them, we show that the controlled dynamics can be represented as a transition between a pair of time-dependent states [26].

A. Coarse-Grained Rabi State and Frequency

As shown in Sec. II A, the overlap in the controlled dynamics rapidly oscillates because the system contains many states. To analyze this complicated behavior more easily, we introduce the following two time-dependent

states,

$$|\phi_0(t)\rangle = \hat{U}_0(t,0)|\varphi_i\rangle, \quad |\chi_0(t)\rangle = \hat{U}_0(t,T)|\varphi_f\rangle \quad (16)$$

where

$$\hat{U}_0(t_2, t_1) = e^{-iH_0(t_2-t_1)/\hbar} \quad (17)$$

is a “free”-propagator with H_0 from $t = t_1$ to t_2 , and T is a target time. These states are an analogue of eigenstates in the usual Rabi state (15), and we try to describe the controlled dynamics as a transition from $|\phi_0(t)\rangle$ to $|\chi_0(t)\rangle$.

We introduce another quantum state by a linear combination of the two time-dependent states,

$$|\phi(t)\rangle = |\phi_0(t)\rangle c(t) + |\chi_0(t)\rangle s(t) \quad (18)$$

where $c(t)$ and $s(t)$ are functions satisfying a normalization condition:

$$|c(t)|^2 + |s(t)|^2 = 1. \quad (19)$$

If we require $|\phi(t)\rangle$ to satisfy Schrödinger’s equation, we obtain

$$i\hbar \left[|\phi_0(t)\rangle \frac{d}{dt} c(t) + |\chi_0(t)\rangle \frac{d}{dt} s(t) \right] = \varepsilon(t)V [|\phi_0(t)\rangle c(t) + |\chi_0(t)\rangle s(t)]. \quad (20)$$

Multiplying $\langle\phi_0(t)|$ and $\langle\chi_0(t)|$ from the left gives the following equations for $c(t)$ and $s(t)$

$$i\hbar \frac{d}{dt} \begin{pmatrix} c(t) \\ s(t) \end{pmatrix} = \begin{pmatrix} \langle\phi_0(t)|\varepsilon(t)V|\phi_0(t)\rangle & \langle\phi_0(t)|\varepsilon(t)V|\chi_0(t)\rangle \\ \langle\chi_0(t)|\varepsilon(t)V|\phi_0(t)\rangle & \langle\chi_0(t)|\varepsilon(t)V|\chi_0(t)\rangle \end{pmatrix} \begin{pmatrix} c(t) \\ s(t) \end{pmatrix}. \quad (21)$$

where we have used

$$|\langle\phi_0(t)|\chi_0(t)\rangle| \ll 1 \quad (22)$$

which is satisfied when $|\varphi_i\rangle$ and $|\varphi_f\rangle$ are random vectors with a large number of elements.

Our aim is not to solve Eq. (21) exactly, but to find a coarse-grained (CG) solution by ignoring rapidly oscillating terms when the target time T is large enough. If we use the well-optimized field $\varepsilon(t)$, we expect that the following condition

$$|\langle\phi_0(t)|\varepsilon(t)V|\phi_0(t)\rangle|, |\langle\chi_0(t)|\varepsilon(t)V|\chi_0(t)\rangle| \ll |\langle\phi_0(t)|\varepsilon(t)V|\chi_0(t)\rangle|, \quad (23)$$

are satisfied for $T \rightarrow \infty$ under the coarse-grained picture. The validity of this condition will be checked in Sec. III B.

Under this condition, we obtain the following simple equations

$$i\hbar \frac{d}{dt} \begin{pmatrix} c(t) \\ s(t) \end{pmatrix} = \begin{pmatrix} 0 & \hbar\Omega \\ \hbar\Omega^* & 0 \end{pmatrix} \begin{pmatrix} c(t) \\ s(t) \end{pmatrix}, \quad (24)$$

where

$$\Omega \equiv \left\langle \frac{\langle\phi_0(t)|\varepsilon(t)V|\chi_0(t)\rangle}{\hbar} \right\rangle_{\text{CG}} \quad (25)$$

is a frequency defined by ignoring rapidly oscillating terms. We also expect that Ω has a constant (time-independent) value, which will be justified below. Then, the boundary conditions $c(0) = 1$ and $s(0) = 0$ gives a solution

$$c(t) = \cos |\Omega|t, \quad s(t) = -ie^{-i\theta} \sin |\Omega|t \quad (26)$$

where $e^{i\theta} = \Omega/|\Omega|$. The final expression of the controlled dynamics is

$$|\phi(t)\rangle = |\phi_0(t)\rangle \cos |\Omega|t - ie^{-i\theta} |\chi_0(t)\rangle \sin |\Omega|t. \quad (27)$$

Note that this state is interpreted to represent a transition between $|\phi_0(t)\rangle$ and $|\chi_0(t)\rangle$ or that between $|\varphi_i\rangle$ and $|\varphi_f\rangle$. Since this is very similar to the usual Rabi state, Eq. (15), we call this state, Eq. (27), “CG Rabi state”, and the frequency, Eq. (25), “CG Rabi frequency”.

B. Actual Coarse-Graining Procedure

In the previous subsection, we have introduced the concept “coarse-graining” (CG) to define the CG Rabi frequency Ω , Eq. (25). In the actual calculations, we carry out this procedure by averaging over a certain time interval,

$$\langle A(t) \rangle_{\text{CG}} \equiv \frac{1}{t_2 - t_1} \int_{t_1}^{t_2} A(t') dt'. \quad (28)$$

Though this result depends on the choice of t_1, t_2 in general, we consider that there exists a natural time scale where the time averaging is meaningful. In optimal

control problems, if we choose the target time T large enough, we can substitute the range of the integration into above expression, i.e., $t_1 = 0$ to $t_2 = T$.

To check when the condition, Eq. (23), is fulfilled, and when the CG Rabi frequency Ω defined in Eq. (25) becomes constant, we introduce the following integrals

$$F(t) = \int_0^t \langle \phi_0(t') | \varepsilon(t') V | \chi_0(t') \rangle dt' \quad (29)$$

$$g_\phi(t) = \int_0^t \langle \phi_0(t') | \varepsilon(t') V | \phi_0(t') \rangle dt' \quad (30)$$

$$g_\chi(t) = \int_0^t \langle \chi_0(t') | \varepsilon(t') V | \chi_0(t') \rangle dt'. \quad (31)$$

Though the integrands are rapidly oscillating, a certain smoothness can be observed in those integrals, especially for $F(t)$. In such a case, we judge that ‘‘coarse-graining’’ (CG) is appropriate. Note that $F(t)$ is a linear function of t when the CG Rabi frequency Ω is constant.

Figure 6 shows $|F(t)|$, $|g_\phi(t)|$, and $|g_\chi(t)|$ obtained from the numerical results in Sec. II A. For the case of $T = 20$ in Fig. 6(a), the values of $g_\phi(t)$ and $g_\chi(t)$ are small compared to $F(t)$, but $F(t)$ cannot be considered as a linear function of t . Thus, CG is not appropriate in this case. On the other hand, examining the case of $T = 200$ in Fig. 6(b), we realize that the condition, Eq. (23), is satisfied, and $F(t)$ is regarded as a linear function of t . Hence we conclude that CG for random matrix systems is appropriate for a rather large target time T , and in such a case, the CG Rabi frequency becomes constant.

C. Smooth Transition between Random Vectors

In Sec. II A, we have already obtained the optimal field $\varepsilon(t)$ by the numerical calculation for the random matrix systems, Eq. (7). However, only the overlap between the time-evolving controlled state $|\phi(t)\rangle$ and the target state $|\varphi_f\rangle$ was shown there. In this section, we show the overlaps between the time-dependent states defined by Eq. (16) and $|\phi(t)\rangle$, and find a smooth transition picture.

In Fig. 7(a), we show the overlap $|\langle \phi_0(t) | \phi(t) \rangle|^2$ and $|\langle \chi_0(t) | \phi(t) \rangle|^2$ which are obtained from the dynamics driven by the same external field shown in Fig. 1(a). Those curves in the figure are not smooth, and it seems to be difficult to approximate them by the CG Rabi state, Eq. (27), with a constant Ω . In Fig. 7(b), on the other hand, we see a smooth transition from $|\phi_0(t)\rangle$ to $|\chi_0(t)\rangle$, which is induced by the optimal field shown in Fig. 2(a). In this case, the dynamics can be well represented by the CG Rabi state with a constant Ω .

IV. ANALYTIC EXPRESSION FOR THE OPTIMAL FIELD

In the previous sections, we have studied the controlled dynamics when an optimal field is first given by the ZBR-

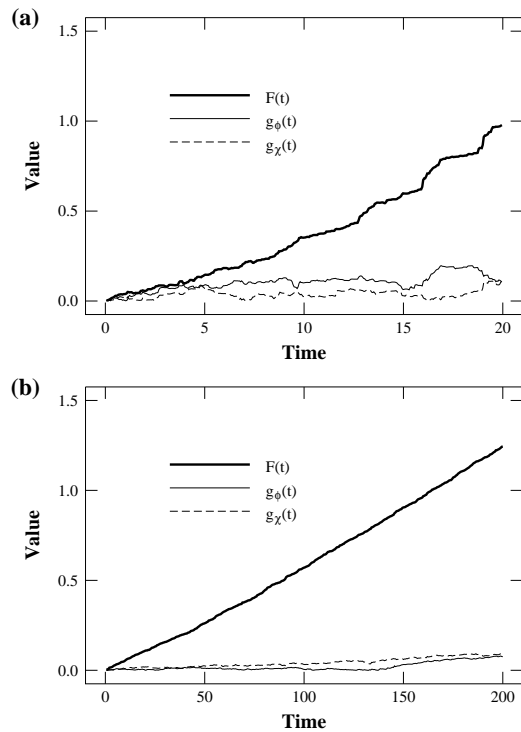


FIG. 6: Absolute values of the functions $F(t)$, $g_\phi(t)$, and $g_\chi(t)$ (see the main text) are shown: (a) $T = 20$ and $\alpha = 1$; (b) $T = 200$ and $\alpha = 10$. The external fields used in these calculations are already shown in Fig. 1(a) and Fig. 2(a), respectively.

OCT scheme. In this section, in turn, we first assume that the dynamics is well approximated by the CG Rabi state, and try to derive an analytic optimal field by using OCT [26].

A. Coarse-Grained Transition Element

We start from an assumption that optimally controlled quantum states are represented by the CG Rabi states, i.e., the forwardly evolving state $|\phi(t)\rangle$ and the inversely evolving state $|\chi(t)\rangle$ are assumed to be

$$\begin{aligned} |\phi(t)\rangle &= |\phi_0(t)\rangle \cos |\Omega|t - ie^{-i\theta} |\chi_0(t)\rangle \sin |\Omega|t \quad (32) \\ |\chi(t)\rangle &= -ie^{i\theta} |\phi_0(t)\rangle \sin |\Omega|(t-T) \\ &\quad + |\chi_0(t)\rangle \cos |\Omega|(t-T). \quad (33) \end{aligned}$$

As we have seen numerically in Sec. III C, the optimal field induces a smooth transition between $|\phi_0(t)\rangle$ and $|\chi_0(t)\rangle$. In this section, we employ OCT to study an analytic formulation of the optimal field. Substituting Eqs. (32) and (33) into the expression of the optimal field, Eq. (6), and after some manipulations, we obtain

$$\varepsilon(t) = \frac{\sin 2|\Omega|T}{2\alpha\hbar} \text{Re} [e^{-i\theta} \langle \phi_0(t) | V | \chi_0(t) \rangle], \quad (34)$$

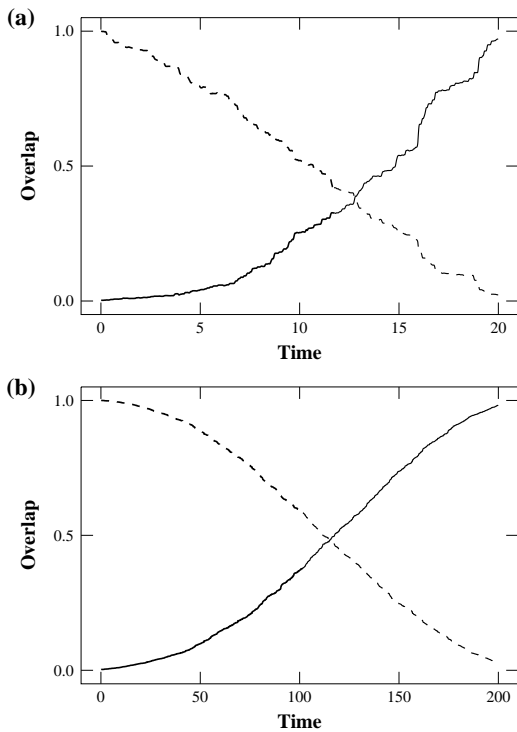


FIG. 7: The overlaps $|\langle\phi_0(t)|\phi(t)\rangle|^2$ and $|\langle\chi_0(t)|\phi(t)\rangle|^2$ are shown: (a) $T = 20$ and $\alpha = 1$; (b) $T = 200$ and $\alpha = 10$. The external fields used in these calculations are already shown in Fig. 1(a) and Fig. 2(a), respectively.

where $|\langle\phi_0(t)|\chi_0(t)\rangle| \ll 1$ has been used as before. This is an analytic expression for the optimal field while the value of the CG Rabi frequency Ω and the phase parameter θ have not been determined yet.

The definition of the CG Rabi frequency, Eq. (25), is used to determine $|\Omega|$. Substituting Eq. (34) and using the relation $\Omega = e^{i\theta}|\Omega|$, we obtain

$$|\Omega| = \frac{\bar{V}^2 \sin 2|\Omega|T}{4\alpha\hbar^2} \quad (35)$$

where

$$\bar{V}^2 \equiv \left\langle |\langle\phi_0(t)|V|\chi_0(t)\rangle|^2 + [e^{-i\theta}\langle\phi_0(t)|V|\chi_0(t)\rangle]^2 \right\rangle_{\text{CG}} \quad (36)$$

is a CG transition element. This equation gives $|\Omega|$ when the penalty factor α and the target time T are fixed. For a large T , the second term in the right-hand side is considered small compared to the first term. In order to see this, we represent the initial and final state using the eigenstates $|\phi_k\rangle$ of H_0 as

$$|\varphi_i\rangle = \sum_j c_j |\phi_j\rangle, \quad |\varphi_f\rangle = \sum_k d_k |\phi_k\rangle, \quad (37)$$

with the coefficients c_j and d_j . For a large T , we can

ignore oscillating terms to obtain

$$\begin{aligned} |\langle\phi_0(t)|V|\chi_0(t)\rangle|^2 &= \sum_{j,k} |c_j|^2 |V_{jk}|^2 |d_k|^2 + |R(T)|^2 \end{aligned} \quad (38)$$

$$|\langle\phi_0(t)|V|\chi_0(t)\rangle|^2 = (R(T))^2 \quad (39)$$

where

$$R(T) \equiv \sum_j c_j^* V_{jj} d_j e^{-E_j T / i\hbar}, \quad (40)$$

becomes small for $N \rightarrow \infty$ when $|\varphi_i\rangle$ and $|\varphi_f\rangle$ are random vectors without any special correlation. Thus Eq. (35) is simplified as

$$\bar{V}^2 \approx \sum_{j,k} |c_j|^2 |V_{jk}|^2 |d_k|^2. \quad (41)$$

If the following condition

$$\frac{\bar{V}^2 T}{2\alpha\hbar^2} > 1, \quad (42)$$

is satisfied, at least one $|\Omega|$ ($\Omega \neq 0$) is obtained from Eq. (35). Using this $|\Omega|$, the final overlap J_0 is given by

$$J_0 = \sin^2 |\Omega|T, \quad (43)$$

and the averaged amplitude $\bar{\varepsilon}$ of the external field (34) is calculated as

$$\bar{\varepsilon} \equiv \sqrt{\frac{1}{T} \int_0^T |\varepsilon(t)|^2 dt} \approx \frac{\sqrt{2}\hbar|\Omega|}{V}. \quad (44)$$

In Fig. 8, we compare the predicted values, Eqs. (43) and (44), with the numerical results for the random matrix system. Those results agree well each other especially for a large T , i.e., the CG picture is valid and useful especially for a large target time T . [37]

B. Analytic Solution for Perfect Control

In the ZBR scheme, we must choose a small penalty factor α to make the final overlap large enough. In our analytical results, if we take the limit $\alpha \rightarrow 0$, we find that

$$|\Omega| = \frac{(2k-1)\pi}{2T} \quad (k = 1, 2, \dots) \quad (45)$$

satisfies Eq. (35), and then $J_0 = 1$, i.e., a perfect control is achieved. Using Eqs. (34) and (35), the optimal field for the perfect control in the small α limit is obtained as

$$\varepsilon(t) = \frac{(2k-1)\pi\hbar}{\bar{V}^2 T} \text{Re} [e^{-i\theta} \langle\phi_0(t)|V|\chi_0(t)\rangle] \quad (46)$$

where θ can be determined by a normalization condition as

$$e^{2i\theta} = \frac{\langle\phi_0(T)|\varphi_f\rangle}{\langle\varphi_f|\phi_0(T)\rangle}. \quad (47)$$

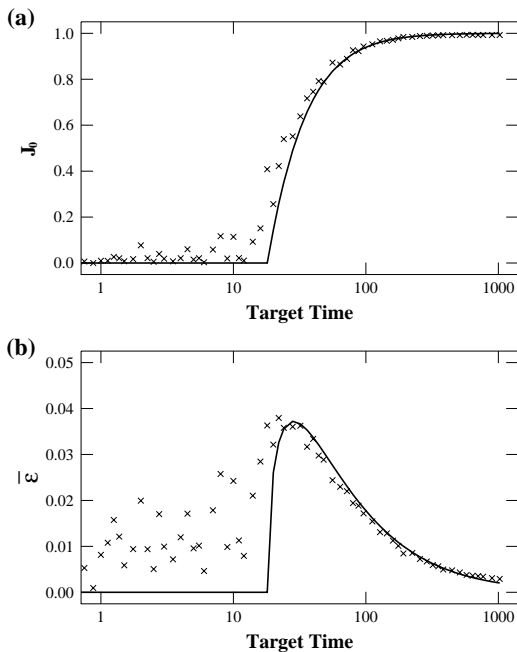


FIG. 8: (a) The final overlap $J_0 = |\langle \phi(T) | \varphi_f \rangle|^2$ and (b) the averaged field amplitude $\bar{\epsilon}$ for a 64×64 random matrix system are shown as a function of the target time T . Marks (\times) represent the numerical results by the Zhu-Botina-Rabitz scheme. Solid curves represent our analytic results under the assumption of the CG Rabi state.

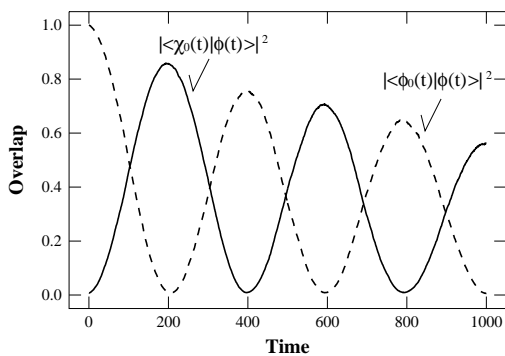


FIG. 9: The coarse-grained Rabi oscillation induced by the analytical external field for perfect control is shown for the case $k = 3$ in Eq. (46). The solid curve represents $|\langle \chi_0(t) | \phi(t) \rangle|^2$, and the dashed $|\langle \phi_0(t) | \phi(t) \rangle|^2$. The initial and the target states are Gaussian random vectors in a 256×256 GOE random matrix Hamiltonian system.

This field is expected to be the optimal field which steers the quantum state $|\varphi_i\rangle$ at $t = 0$ to $|\varphi_f\rangle$ at $t = T$, as well as it induces a CG Rabi oscillation between $|\phi_0(t)\rangle$ and $|\chi_0(t)\rangle$. Note that the penalty factor α does not appear in Eq. (46), so this is different from other non-iterative optimal fields discussed in [15].

We next examine when and how the analytic opti-

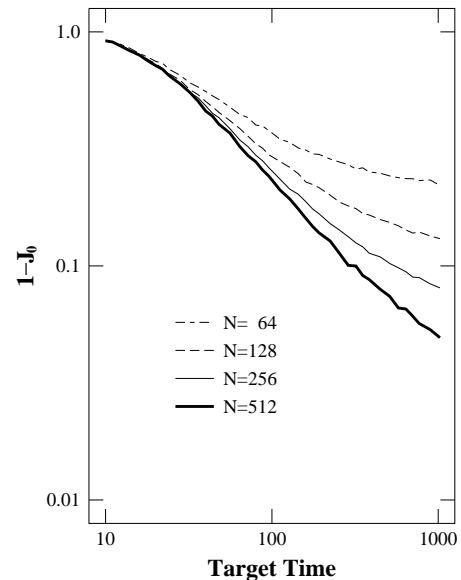


FIG. 10: The target-time dependence of the final overlap J_0 by the analytic optimal field with $k = 1$ is shown. The residual probability $1 - J_0$ from the perfect control $J_0 = 1$ is depicted for various matrix sizes N of GOE random Hamiltonians. The initial and the final states are Gaussian random vectors.

mal field works for a random matrix system (256×256 GOE random matrix). Figure 9 demonstrates the coarse-grained Rabi oscillation induced by the analytic field, Eq. (46), with $k = 3$, where smooth oscillations of $|\langle \phi_0(t) | \phi(t) \rangle|^2$ and $|\langle \chi_0(t) | \phi(t) \rangle|^2$ are observed. The initial and the target states are both Gaussian random vectors with 256 elements. This result shows that the field actually produces the CG Rabi oscillation in the random matrix system.

Finally, in Fig. 10, we show the performance of the analytic field, Eq. (46), for the same type of control problem with various matrix sizes. The abscissa and the ordinate are the target time T and the residual probability $1 - J_0$, respectively. This result shows that the final overlap J_0 approaches unity, i.e., the perfect control is achieved as the target time and the matrix size become both large.

V. SUMMARY AND DISCUSSION

We have studied optimal control of random matrix systems and a quantum kicked rotor as examples of quantum chaos systems. Using the ZBR-OCT scheme, we numerically achieved almost perfect control for the above systems where the initial state $|\varphi_i\rangle$ and the target state $|\varphi_f\rangle$ are random vectors (except the case of a quantum kicked rotor with $K = 1$). However, the optimal fields and the overlap $|\langle \phi(t) | \varphi_f \rangle|^2$ thus obtained are too complicated to be analyzed as shown in Figs. 1, 2, 3, and 4. On the other hand, as shown in Fig. 7,

the overlaps $|\langle\phi_0(t)|\phi(t)\rangle|^2$ and $|\langle\chi_0(t)|\phi(t)\rangle|^2$ are rather smooth where $|\phi_0(t)\rangle$ ($|\chi_0(t)\rangle$) represents a free forward (backward) evolution of the system, so we can introduce coarse grained concepts: a CG Rabi state and a CG Rabi frequency. The CG Rabi state is an analogue of a usual Rabi state but it describes a transition between $|\phi_0(t)\rangle$ and $|\chi_0(t)\rangle$ as in Eq. (27). The CG Rabi frequency is defined by ignoring rapidly oscillating terms as in Eq. (25). We applied this picture to OCT and obtained an analytic expression for the optimal field, Eq. (46). We also numerically confirmed that the analytic field actually works in controlling random vectors when the target time and the matrix size are both large enough.

In closing, we discuss future directions of this study: (a) We mainly studied strong-chaos limit cases as described by random matrix Hamiltonians, and applied the coarse grained ideas to them. Thus, the next problem should be addressed on less chaotic cases as described by banded random matrix Hamiltonians. A quantum kicked rotor with a small K will be a good example for that purpose [27]. (b) The other interesting prob-

lem is the semiclassical limit of the controlled dynamics. Though we have shown that quantum chaos systems can be controlled, we don't know its semiclassical behavior since there are many difficulties in taking the semiclassical limit $\hbar \rightarrow 0$. There are, on the other hand, many works studying *chaos control* in classical mechanics, and there are some examples utilizing stochastic features of phase space in "targeting" problems [28, 29]. In this respect, it is strongly desirable to study chaos control from semiclassical points of view [30, 31]. (c) In connection with quantum information processings, control of quantum entanglement in quantum chaos systems [32] will be another interesting subject to be pursued.

Acknowledgments

The authors thank Prof. S. A. Rice, Prof. H. Rabitz, Prof. M. Toda, Prof. H. Nakamura, Prof. H. Kono, Prof. S. Tasaki, Prof. A. Shudo, Dr. Y. Ohtsuki, and Dr. G. V. Mil'nikov for useful discussions.

-
- [1] M. A. Nielsen and I. L. Chuang, *Quantum Computation and Quantum Information* (Cambridge University Press, Cambridge, 2000).
- [2] V. Ramakrishna and H. Rabitz, "Relation between quantum computing and quantum controllability," *Phys. Rev. A* **54**, 1715 (1996).
- [3] C. M. Tesch and R. de Vivie-Riedle, "Quantum Computation with Vibrationally Excited Molecules," *Phys. Rev. Lett.* **89**, 157901 (2002); J. P. Palao and R. Kosloff, "Quantum Computing by an Optimal Control Algorithm for Unitary Transformations," *ibid.* **89**, 188301 (2002).
- [4] S. A. Rice and M. Zhao, *Optical Control of Molecular Dynamics* (John Wiley & Sons, New York, 2000).
- [5] L. Allen and J. H. Eberly, *Optical Resonance and Two-level Atoms* (Dover, New York, 1987).
- [6] J. S. Melinger, S. R. Gandhi, A. Hariharan, D. Goswami, and W. S. Warren, "Adiabatic population transfer with frequency-swept laser pulses," *J. Chem. Phys.* **101**, 6439 (1994).
- [7] Y. Teranishi and H. Nakamura, "Control of Time-Dependent Nonadiabatic Processes by an External Field," *Phys. Rev. Lett.* **81**, 2032 (1998); K. Nagaya, Y. Teranishi and H. Nakamura, "Control of molecular processes by a sequence of linearly chirped pulses," *J. Chem. Phys.* **117**, 9588 (2002); H. Fujisaki, Y. Teranishi and H. Nakamura, "Control of photodissociation branching using the complete reflection phenomenon: Application to HI molecule," *J. Theor. Comp. Chem.* **1**, 245 (2002).
- [8] K. Bergmann, H. Theuer, and B. W. Shore, "Coherent population transfer among quantum states of atoms and molecules," *Rev. Mod. Phys.* **70**, 1003 (1998).
- [9] D. J. Tannor and S. A. Rice, "Control of selectivity of chemical reaction via control of wave packet evolution," *J. Chem. Phys.* **83**, 5013 (1985).
- [10] M. Shapiro and P. Brumer, "Laser control of product quantum state populations in unimolecular reactions," *J. Chem. Phys.* **84**, 4103 (1986); M. Shapiro and P. Brumer, *Principles of the Quantum Control of Molecular Processes* (John Wiley & Sons, New York, 2003).
- [11] G. M. Huang, T. J. Tarn, and J. W. Clark, "On the controllability of quantum-mechanical systems," *J. Math. Phys.* **24**, 2608 (1983).
- [12] A. P. Peirce, M. A. Dahleh, and H. Rabitz, "Optimal control of quantum-mechanical systems: Existence, numerical approximation, and applications," *Phys. Rev. A* **37**, 4950 (1988).
- [13] W. Zhu, J. Botina, and H. Rabitz, "Rapidly Convergent Iteration Methods for Quantum Optimal Control of Population," *J. Chem. Phys.* **108**, 1953 (1998).
- [14] R. S. Judson and H. Rabitz, "Teaching Lasers to Control Molecules," *Phys. Rev. Lett.* **68**, 1500 (1992).
- [15] W. Zhu and H. Rabitz, "Noniterative algorithms for finding quantum optimal controls," *J. Chem. Phys.* **110**, 7142 (1999).
- [16] M. C. Gutzwiller, *Chaos in Classical and Quantum Mechanics* (Springer-Verlag, New York, 1990).
- [17] F. Haake, *Quantum Signatures of Chaos*, 2nd Edition (Springer-Verlag, Heidelberg, 2001).
- [18] P. Gaspard, S. A. Rice, H. J. Mikeska, and K. Nakamura, "Parametric motion of energy levels: Curvature distribution," *Phys. Rev. A* **42**, 4015 (1990).
- [19] T. Takami, "Curvature distribution of stadium billiard," *J. Phys. Soc. Jpn.* **60**, 2489 (1991); T. Takami and H. Hasegawa, "Curvature distribution of chaotic quantum systems: Universality and nonuniversality," *Phys. Rev. Lett.* **68**, 419 (1992).
- [20] J. Zakrzewski and D. Delande, "Parametric motion of energy levels in quantum chaotic systems. I. Curvature

- distributions,” *Phys. Rev. E* **47**, 1650 (1993).
- [21] T. Takami, “Semiclassical interpretation of avoided crossings for classically nonintegrable systems,” *Phys. Rev. Lett.* **68**, 3371 (1992); T. Takami, “Semiclassical study of avoided crossings,” *Phys. Rev. E* **52**, 2434 (1995).
- [22] F. M. Izrailev, “Limiting quasienergy statistics for simple quantum systems,” *Phys. Rev. Lett.* **56**, 541 (1986).
- [23] S.-J. Chang and K.-J. Shi, “Evolution and exact eigenstates of a resonant quantum system,” *Phys. Rev. A* **34**, 7 (1986).
- [24] K. Takahashi, “Distribution Functions in Classical and Quantum Mechanics,” *Prog. Theor. Phys. Suppl.* **98**, 109 (1989).
- [25] T. Takami, H. Fujisaki, and T. Miyadera, “Optimal Control of Quantum Chaotic Dynamics,” unpublished.
- [26] T. Takami and H. Fujisaki, “Coarse Grained Picture for Controlling “Complex” Quantum Systems,” e-print nlin.CD/0402003, submitted to *Phys. Rev. Lett.*
- [27] Coherent control of a quantum kicked rotor was studied in J. Gong and P. Brumer, “Coherent Control of Quantum Chaotic Diffusion,” *Phys. Rev. Lett.* **86**, 1741 (2001); “Coherent control of quantum chaotic diffusion: Diatomic molecules in a pulsed microwave field,” *J. Chem. Phys.* **115**, 3590 (2001).
- [28] E. Ott, *Chaos in Dynamical Systems*, 2nd Edition (Cambridge University Press, Cambridge, 2002); T. Shinbrot, E. Ott, C. Grebogi, and J. A. Yorke, “Using chaos to direct trajectories to targets,” *Phys. Rev. Lett.* **65**, 3215 (1990).
- [29] C. D. Schwieters and H. Rabitz, “Optimal control of nonlinear classical systems with application to unimolecular dissociation reactions and chaotic potentials,” *Phys. Rev. A* **44**, 5224 (1991); J. Botina, H. Rabitz, and N. Rahman, “Optimal control of chaotic Hamiltonian dynamics,” *Phys. Rev. A* **51**, 923 (1995).
- [30] V. S. Batista and P. Brumer, “Coherent control in the presence of intrinsic decoherence: Proton transfer in large molecular systems,” *Phys. Rev. Lett.* **89**, 143201 (2002).
- [31] H. Fujisaki, Y. Teranishi, A. Kondorskiy, and H. Nakamura, “Semiclassical approaches to controlling chemical reaction dynamics,” e-print quant-ph/0302025.
- [32] A. Tanaka, H. Fujisaki, and T. Miyadera, “Saturation of the production of quantum entanglement between weakly coupled mapping systems in strongly chaotic region,” *Phys. Rev. E* **66**, 045201(R) (2002); H. Fujisaki, T. Miyadera, and A. Tanaka, “Dynamical aspects of quantum entanglement for weakly coupled kicked tops,” *Phys. Rev. E* **67**, 066201 (2003).
- [33] In numerical studies below, we obtain such vectors with normalization after generating random complex elements subject to the distribution.
- [34] In the insets of Figs. 1(c) and 2(c), we show the overlaps $|\langle\phi(t)|\varphi_f\rangle|^2$ near $t = T$ in a magnified scale. They exhibit almost the same curves in spite of the different optimal fields. This is because the optimal field is small enough so that the dynamics is not affected in this time scale.
- [35] We use the parameters $N = 128$ and $M = 7$. Thus the quantum states are represented by 128 discrete points, and the range of momentum is from -7π to 7π . The value of $\hbar = 2\pi M/N$ is 0.3436.
- [36] When the control purpose is to steer a wavepacket in a torus to another place in another torus, OCT fails. This is because the wavepacket is trapped in one torus and it is very hard to escape from the torus with a weak external field.
- [37] Note that there exists a threshold $T_c \equiv 2\alpha\hbar^2/\bar{V}^2$, the smallest target time satisfying the condition, Eq. (42). If we choose a smaller T than T_c , there is no external field which induces the smooth transition described by the CG Rabi state. On the other hand, the numerical method can give finite solutions for such cases because there is no assumption (restriction) about the dynamics except that it obeys to the Schrödinger equation.